IN-PLANE AND OUT-OF-PLANE INSTABILITY OF A 297 M SPAN STEEL ARCH BRIDGE

Yukio Maeda and Masa Hayashi, Osaka University, Japan

Ohmishima Bridge, which is now under construction in Japan, is a steel highway bridge spanning 297 m (974.4ft.) of a half-through two-hinged solid rib arch stiffened by side ties. The two main arch ribs of box section are stiffened respectively, by two side ties. One end of each tie is fixed to the top of an abutment in both side spans. Bending moments and stresses due to live loads or wind loads in the arch ribs can be reduced by the stiffening ties more than those of ordinary two-hinged arches, and the steel weight of the ribs decreases considerably. Therefore, this new type arch is more economical than an ordinary two-hinged or fixed solid rib arch. Since the arch ribs become more slender, geometrical nonlinearity of the arch may be more remarkable. To investigate the geometrical and material nonlinearities of such a long-span and unusual type of steel arch bridge including overall inelastic instability, extensive experimental and analytical studies were carried out. In this paper, the results of the analytical study with discussions are reported. The combined nonlinear analyses are performed by a matrix method based on finite displacement theory for in-plane and out-of-plane instability. It was confirmed that the side ties for stiffening a two-hinged arch bridge are very effective for the reduction of stresses and geometrical nonlinearities and for an increase of overall ultimate strength in-plane or out-of-plane of the arch.

Ohmishima Bridge is now under construction in Japan as the first bridge of long-span bridge projects to connect the Mainland to Shikoku Island crossing the Seto Inland Sea. It is a half-through highway bridge spanning 297 m (974.4 ft.) of a two-hinged steel arch stiffened by side ties, which may be called a new type of arch bridge not experienced in the world.

The first design proposed for *Ohmishima Bridge* was a fixed steel arch bridge(1), but it was changed into the present final design of a new type of two-hinged arch. Since smaller box sections can be used for its arch ribs due to reduced bending moments, this type of bridge gives a more economical and rational design than a fixed arch bridge or an ordinary two-hinged arch bridge. However, its more slender arch ribs may cause greater nonlinear structural behaviors.

In this paper, a theoretical study on this new type of arch bridge modelling *Ohmishima Bridge* will be presented(2). The geometrical nonlinear behaviors under design loads and the ultimate strength are investigated in terms of in-plane and out-of-plane instability. First of all, the outline of analytical method by a matrix method based on finite displacement theory will be shown. Then, the calculation results will be discussed on the characteristics of structural behaviors.

The three-dimensional nonlinear analysis of framed structures considering finite rotations of displacement components has not been reported. Also, the elasto-plastic space analysis taking account of the effects of finite rotations and spread of plastic region in the whole members has not been applied to an actual bridge. Therefore, these effects are considered as accurately as possible in numerical calculations by means of theoretical analysis and numerical computation.

Summary of Nonlinear Analysis

Nonlinear analyses of the arch are carried out by a matrix method based on finite displacement theory. An outline of analytical methods for space frames is given as follows, except the planer analysis.

Assumptions

The following assumptions are imposed in the combined nonlinear analysis of space frames:

1. Members are straight thin-walled beams of a doubly symmetrical uniform cross-section.
2. The longitudinal dimension of a beam is much larger than its lateral dimension.
3. The middle line of thin walls in a cross section does not distort after the deformation of the beam.
4. Thin walls deform under the Kirchhoff-Love hypothesis for thin shells.
5. Warping of cross sections, shear distortion, overall buckling of members and local buckling of thin walls are ignored.
6. The Mises yield condition and the Prandtl-Reuss equation are employed in plastic regions of walls.
7. The stress-strain diagram of material is assumed to be linearly elastic-perfectly plastic.

Finite Displacement of Beam

Finite rotations in a three-dimensional space do not satisfy a commutative law, nevertheless they have been treated as a vector in most studies(3, 4). In space analysis, only Oran(5) pointed out the above-mentioned misunderstanding and used a rotation matrix which was called a joint orientation matrix in his paper. However, the rotation matrix shown in his paper is one for a small rotation.

A rotation matrix of a nodal point was formularized(6) with a coordinate transformation matrix of a member taking account of finite rotations as well as finite translations. These matrices are mathematically exact ones.

Figure 1. Local coordinate systems of a member.

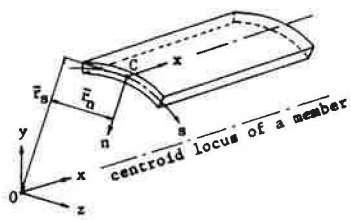

By the use of this rotation matrix, the finite displacements $\bar{u}$, $\bar{v}$ and $\bar{w}$ of an arbitrary point C on the middle surface of a thin wall are obtained under the assumption 3. They are expressed by omitting nonlinear terms higher than the third order as follows:

$$\bar{u} = u_0 - v_0'\bar{y} - w_0'\bar{z} - \frac{1}{2}\phi_0(w_0'\bar{y} - v_0'\bar{z}), \tag{1}$$

$$\bar{v} = v_0 - \phi_0\bar{z} - \frac{1}{2}[\phi_0^2\bar{y} + (v_0')^2\bar{y} + v_0'w_0'\bar{z}], \tag{2}$$

$$\bar{w} = w_0 + \phi_0\bar{y} - \frac{1}{2}[\phi_0^2\bar{z} + (w_0')^2\bar{z} + v_0'w_0'\bar{y}] \tag{3}$$

where u_0, v_0, w_0 are the displacement components and ϕ_0 the torsional angle at the centroid O of a cross section having the coordinates $(x, 0, 0)$ in a rectangular Cartesian coordinate system (x, y, z). $\bar{y}$ and $\bar{z}$ are the coordinates of the point C, and the prime superscript indicates differentiation with respect to x.

Strains of Thin Wall

The strains and the stresses of a thin wall are expressed in a local system of orthogonal curvilinear coordinates (x, s, n) at the point C.

Strain components are obtained by using the displacements of equations 1, 2 and 3 on the middle surface of the wall under the Kirchhoff-Love hypothesis(7).

The Lagrangian strain components of e_{ss}, e_{nn}, e_{xn} and e_{sn} may be ignored due to the assumptions 3 and 4:

$$e_{ss} = e_{nn} = e_{xn} = e_{sn} = 0. \tag{4}$$

The other components can be written in terms of the displacement components at the centroid O as follows:

$$\begin{aligned} e_{xx} = {} & u_0' - (v_0''\bar{y} + w_0''\bar{z}) + \frac{1}{2}[(u_0')^2 + (v_0')^2 + (w_0')^2] \\ & - \frac{1}{2}(\phi_0 w_0'' - \phi_0' w_0' + 2u_0'v_0'')\bar{y} + \frac{1}{2}(v_0''\bar{y} + w_0''\bar{z})^2 \\ & + \frac{1}{2}(\phi_0 v_0'' - \phi_0' v_0' - 2u_0'w_0'')\bar{z} + \frac{1}{2}(\phi_0')^2(\bar{y}^2 + \bar{z}^2) \\ & + [(v_0''\sin\beta - w_0''\cos\beta) - \phi_0''\bar{r}_n]n \end{aligned} \tag{5}$$

$$\begin{aligned} 2e_{xs} = {} & [\phi_0'\bar{r}_s + \frac{1}{2}(v_0''w_0' - v_0'w_0'')\bar{r}_s + \frac{1}{2}\phi_0(w_0'\cos\beta \\ & - v_0'\sin\beta) - u_0'(v_0'\cos\beta + w_0'\sin\beta)](1 - n/R)^{-1} \\ & - 2\phi_0'n \end{aligned} \tag{6}$$

where β is the angle between y-axis and t-axis which is the tangent at C to the curvilinear coordinates s; R is the radius of curvature of the wall in the direction n; and $\bar{r}_s$ and $\bar{r}_n$ are given by the following expressions:

$$\bar{r}_s = \bar{y}\sin\beta - \bar{z}\cos\beta, \quad \bar{r}_n = \bar{y}\cos\beta + \bar{z}\sin\beta. \tag{7}$$

According to the assumption of thinness of a wall, the nonlinear terms with respect to the n-axis are ignored in equations 5 and 6.

Stresses of Thin Wall

By virtue of the assumptions 3 and 4 about beam theory and thin-shell theory, respectively, only two strain components of equations 5 and 6 will be considered in the nonlinear analysis of a thin-walled member and are expressed by the notations ε and γ, respectively.

Let the stress components corresponding to the above strains be σ and τ, the incremental stress-strain relations are expressed as follows:

$$\begin{Bmatrix} \Delta\sigma \\ \Delta\tau \end{Bmatrix} = \begin{bmatrix} D_1 & D_3 \\ D_3 & D_2 \end{bmatrix} \begin{Bmatrix} \Delta\varepsilon \\ \Delta\gamma \end{Bmatrix} \tag{8}$$

where the notation Δ indicates the increments and D_1, D_2 and D_3 are given for elastic materials with Young's modulus E and shear modulus G

$$D_1 = E, \quad D_2 = G, \quad D_3 = 0, \tag{9}$$

and for plastic materials under the assumptions 6 and 7(8)

$$\left.\begin{aligned} D_1 &= 9EG\tau^2/D_0, \quad D_2 = EG\sigma^2/D_0, \\ D_3 &= -3EG\sigma\tau/D_0, \quad D_0 = E\sigma^2 + 9G\tau^2. \end{aligned}\right\} \tag{10}$$

To take into account the spreading of plastic region in a member in the directions x and s in the elasto-plastic analysis of framed structures, a thin-walled member is divided into many small elements as shown in Figure 2.

Figure 2. Elements of box beam.

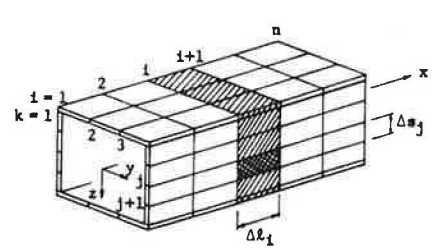

The incremental strain components in plastic regions have a combined effect as expressed by equations 8 and 10. For a thin-walled beam of closed cross section, the incremental shearing stress is obtained by using the shear flow theory which assumes a constant shear flow q in the closed cross section.

The nonlinear terms of the incremental shearing strain may be negligible and a thin-walled beam is assumed to have a box section. Then, the following expression is given by substituting the increments of strain components into equation 8 and by applying linear integration along the closed middle line of the cross section of an elasto-plastic member:

$$\oint \Delta\tau\, ds = \Delta\phi_0' \oint D_2 \bar{r}_s ds + \int_p D_3 \Delta\varepsilon ds \qquad (11)$$

where $\int_p$ implies the integration with respect to plastic regions in the closed cross section.

Let the thickness of a thin wall be t, the incremental shear flow Δq is given by

$$\Delta q = t\Delta\tau , \qquad (12)$$

so that the incremental stress $\Delta\tau_j$ of the j-th element can be obtained by rewriting equation 11 as follows:

$$\Delta\tau_j = \frac{\sum_k (D_2 \bar{r}_s \Delta s)_k}{\sum_k (\Delta s/t)_k} \frac{\Delta\phi_0'}{t_j} + \frac{\sum_p (D_3 \Delta\varepsilon \Delta s)_p}{\sum_k (\Delta s/t)_k} \frac{1}{t_j} \qquad (13)$$

where $\sum_k$ and $\sum_p$ indicate the summation over all elements and over plastic elements alone in a cross section, respectively.

Equilibrium Equations

Equilibrium equations of an elastic or an elasto-plastic member are formularized by the usual matrix method based on the principle of virtual work.

The equations are expressed in terms of matrices as follows:

$$\Delta k \cdot \Delta d = \Delta p - (f - p) \qquad (14)$$

where Δk, Δd, Δp, p and f are the tangential stiffness martix, the incremental displacement vector, the incremental load vector, the total load vector and the internal force vector, respectively.

The matrix Δk and the vector f can be divided into two parts as shown in the following expressions, respectively:

$$\Delta k = k^* - \sum_i k_i^p , \qquad f = f^* - \sum_i f_i^p \qquad (15)$$

where the matrix k^* and the vector f^* are defined for an elastic member or for an elasto-plastic member, of which all elements are assumed to be elastic, and k_i^p and f_i^p are defined for the i-th plastic or unloaded element and respectively equal to a zero matrix and a zero vector for an elastic element.

k^* and f^* are formularized and also k_i^p and f_i^p are calculated not by a numerical integration but by an analytical procedure, so that the computation may be very quick and the numerical solutions may be accurate.

Numerical Procedure

In the numerical analysis, the mixed method of combined Newton-Raphson method with an incremental load or displacement method is used in an elastic range. The increments of external loads or of a component of displacements at a nodal point to control the numerical calculation, are decided automatically in the program so that a few elastic elements in the whole members may yield. Since these increments will be very small quantities, modified incremental method with equilibrium check is used instead of the mixed method in an elasto-plastic range.

The maximum load of a structure is defined by the condition that a structure becomes unstable when the tangential stiffness matrix of the system turns to a negative definite matrix.

Structural Models

Dimensions

Ohmishima Bridge is a stiffening two-hinged solid rib arch as shown in Figure 3, and its overall rigidity is increased by fixing both side ties to each abutment at both side spans. Namely, the arch ribs may be considered to be elastically supported at about one-sixth points of the arch span by triangular frames consisting of an arch rib, a side tie and an abutment. Therefore, the bending moments in the arch ribs can be reduced and improved structural behaviors may be expected at this modified two-hinged arch bridge as if the span length were shortened to two-thirds.

Sectional dimensions of the arch ribs and the other members are shown in Figure 4.

Figure 3. General pictures of Ohmishima Bridge.

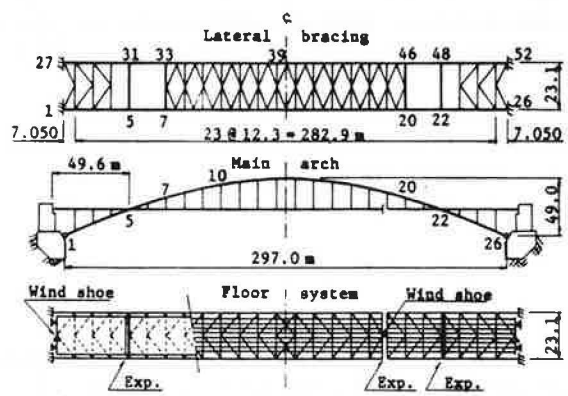

Note: 1 m = 3.28 ft.

Figure 4. Sectional dimensions of members.

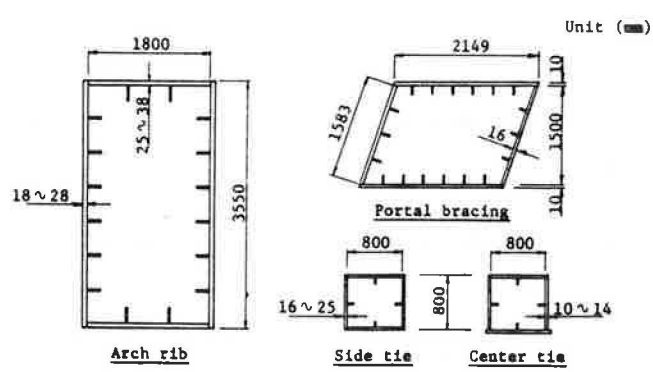

Note: 1 mm = 0.0394 in.

Analytical Models

For a model arch used for in-plane and out-of-plane analyses and elastic and elasto-plastic analyses, the same dimensions as the design of Ohmishima Bridge are used including the condition of supports, the arrangement of expansion joints, the rigidities of members, etc.. To make the calculation simpler, the rigidity of concrete-encased steel grating floor is neglected, eight stringers are replaced by one equivalent stringer, and the arrangement of lateral bracing members between two arch ribs is partly changed. As the result, the model is provided with 139 nodal points and 340 members and is constrainted with 52 degrees of freedom.

In addition to this Model-1, Model-2 is investigated, too, in which either of two side ties is not fixed to the abutment, but supported by a sliding shoe so that the tie is not subjected to any axial force. Moreover, Model-3 with an assumed initial imperfection due to the error of shape in Model-1 is employed in the in-plane ultimate strength analysis.

Applied Loads

In the in-plane analysis, the dead load(D), the live load(L) consisting of uniform load(p) and trailer truck load(TT), both including impact, and the earthquake load(EQ) with the horizontal seismic coefficient of 0.2, are applied at numerical analyses. In the out-of-plane analysis, the dead load, the horizontal earthquake load and wind load(W) are employed.

The intensities of the specific loads like elastic buckling load or ultimate strength load are expressed by a load multiple, α, considering design loads as standard loads, of which the intensities are given in Table 1(2).

Table 1. Intensities of design loads.

Design load	Intensity (kN/m)	Loaded member
Dead load (D)	43.5 94.8 84.8	arch rib center or side tie stringer
Live load (L) (p) (TT)	20.9 765.0(kN)	stringer stringer
Earthquake load (EQ)	8.7 19.0 17.0	arch rib center or side tie stringer
Wind load (W)	19.9 13.0 3.2	arch rib center or side tie post

Note: 1 kN = 0.225 kip. 1 kN/m = 68.5 lbf/ft.

Geometrical Nonlinearity due to In-Plane Loads

Influence Values

To examine the nonlinearity due to live loads, the following five kinds of influence values are considered:

1. An ordinary linear influence value for a unit concentrated load.
2. A linearized influence value for a concentrated live load(TT-Load) obtained by a tangential stiffness matrix at the loading of dead loads.
3. A nonlinear influence value of the exact solution for the value of 2.
4. A linearized influence value for TT-Load obtained by a tangential stiffness matrix at the loading of dead and half-span uniform live loads.
5. A nonlinear influence value of the exact solution for the value of 4.

At the computation of the values of 2 to 5, the exact equilibrium state is obtained for dead loads or plus a uniform live load with the intensities of the design loads. Then, these influence values are calculated not for a unit load, but for TT-Load as a moving concentrated load. At this time, the removal of the linearized errors is tried for bending moments or stresses with the values of 2 and 4.

Nonlinearity due to TT-Load

Figure 5 shows the maximum values of deflections due to a trailer truck load(TT-Load) for Model-1. Figure 6 shows the minimum values of fiber stresses due to TT-Load at the upper and lower flanges for Model-1. Since the linearized influence values of 2 and 4 agree with the values of 3 and 5, respectively, they are not shown in the figures. Those figures indicate clearly the favourable effect of the side ties on the deflections and stresses.

Figure 5. Maximum deflections due to TT-Load.

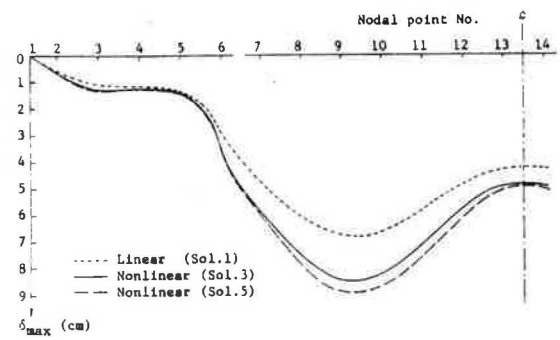

Note: 1 cm = 0.394 in.

Figure 6. Minimum fiber stresses at upper and lower flanges due to TT-Load.

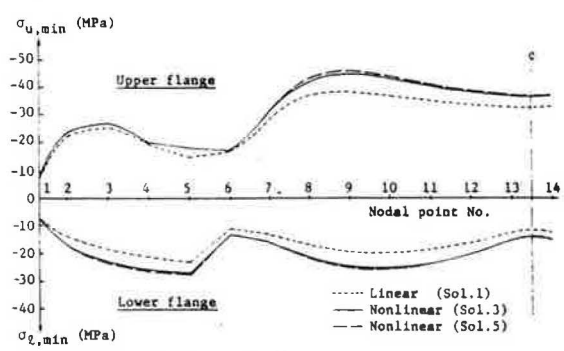

Note: 1MPa = 145 lbf/in^2.

For the maximum or minimum values of deflection δ, bending moment M and fiber stresses σ_u and σ_ℓ in the upper and lower flanges respectively, due to a concentrated TT-Load, the increase ratios of the linearized or the nonlinear values of 2 - 5 to the linear value of 1 are shown in percent on the uppermost column in Table 2.

Table 2. Geometrical nonlinearities of various influence values.

Solution	max δ	max M	min M	min σ_u	min σ_ℓ
Nonlinearity due to TT-Load (%)					
2	25.4	18.8	22.8	17.3	17.0
3	26.4	19.2	22.5	17.8	18.7
4	30.1	21.3	26.3	19.5	19.6
5	31.3	21.7	25.8	20.0	21.4
Nonlinearity due to dead and live loads (%)					
2	6.6	13.4	10.6	4.1	2.2
3	6.9	13.7	10.4	4.3	2.4
4	13.5	22.5	18.9	8.8	5.8
5	13.7	22.7	18.8	8.8	6.0

Since each value shows about 20 - 30% nonlinearity, the linear values cannot be applied to the analysis of the arch. But it may not be required to perform the exact nonlinear calculation for the concentrated live load, as far as the linearized values with 1 - 2% errors are used. When the nonlinear effect due to a uniform live load is taken into account, too, the increase of nonlinearity due to *TT*-Load is about 5% in deflections and about 2- 3% in stresses in comparison of the values of 2 with 4 or the values of 3 with 5.

Nonlinearity due to Dead and Live Loads

Large stresses due to dead loads are observed at a solid rib arch and more than 50% of the stresses are almost axial stresses without nonlinearity. Therefore, nonlinearities due to the dead load plus the live load are indicated on the 2nd column in Table 2, in which the values of 5 give the exact nonlinear effects due to the dead and live loads at Ohmishima Bridge.

Influence Line Analysis

In case that geometrical nonlinearity due to live loads appears at a structure subjected to dead load, an influence line analysis based on the law of superposition cannot be strictly applied to its analysis. Then, an influence line analysis with the above-mentioned influence values of 2 or 3 is applied to the analysis of Model-1.

Table 3. Errors of influence line analysis.

Solution	max δ	max M	min M	min σ_u	min σ_ℓ
Error due to superposition (%)					
2	-2.2	-2.0	-1.2	-1.8	-2.2
3	-1.3	-1.3	-1.2	-1.1	-0.9
Error of influence line analysis (%)					
2	-1.6	-2.0	-1.3	-0.9	-0.9
3	-1.1	-1.5	-1.4	-0.6	-0.5

The value of the uppermost column in Table 3 indicate errors due to the application of the superposition law to the influence analyses of the arch subjected to a uniform live load(p), in terms of the relative errors against the exact values due to the uniform live load.

Furthermore, the errors for the values due to the dead and the uniform live loads are shown on the 2nd column in the table.

The negative signs on the both columns mean unfavorable values.

Effect of Side Ties on Elastic Stability

Load versus displacement curves obtained by a buckling analysis and by an exact finite displacement analysis are given in Figure 7 for the in-plane elastic stability of Model-1 and Model-2 in which the stiffening effect of one of the side ties is neglected. The vertical axis shows load multiples for dead plus live loads and the horizontal axis shows the maximum deflections, both at the nodal point No. 10.

As illustrated in Figure 7, a dynamic jump does not occur at the both models owing to the stiffening effect of the side ties. The comparison between Model-1 and Model-2 shows that the ties have an effect on the constraint of geometrical nonlinearity of the arch. Particularly, the side ties are effective against a seismic load, because the nonlinearity of bending moments due to the dead load plus the seismic load is only 15 - 17% at Model-1, while 60 - 70% at Model-2.

Figure 8 indicates the first mode of buckling due to dead load for Model-1 and -2, in which the left side tie alone is fixed to the abutment. In the figure, the vertical and horizontal axes show relative displacements and nodal point Nos., respectively.

Figure 7. Load versus displacement curves for dead and live loads α (D + L).

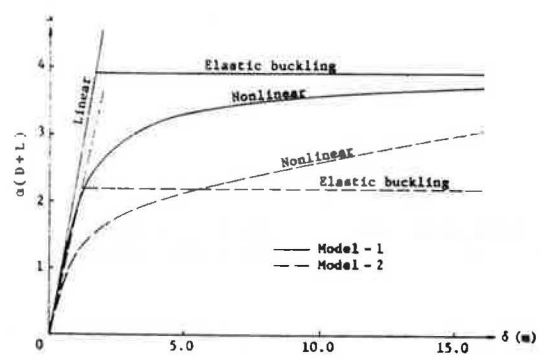

Note: 1 m = 3.28 ft.

Figure 8. Buckling modes due to dead load (α D).

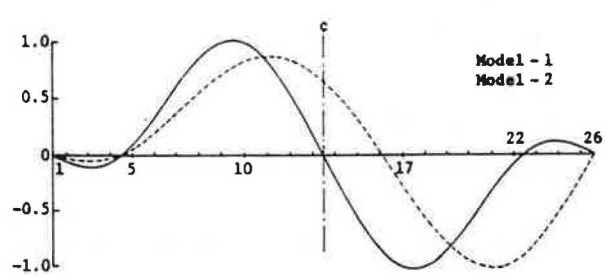

Geometrical Nonlinearity due to Out-of-Plane Loads

Geometrical Nonlinearity

There have been few study reports on the nonlinear behavior of an arch bridge subjected to an out-of-plane load. In Table 4, the geometrical nonlinearities in displacements and internal forces in arch ribs due to design loads calculated by a three-dimensional finite displacement analysis for Model-1 of Ohmishima Bridge, are shown in percent of the linear values. Model-1* in the table is a model arch taking into account the in-plane and out-of-plane rigidities of slab. V and W are respectively vertical and horizontal displacements, N is axial force, and M_t, M_y, M_z are respectively torsional, in-plane, out-of-plane bending moments. It can be seen in Table 4, that the nonlinearities appear even at the design loads, particularly remarkably in the in-plane moments.

Table 4. Geometrical nonlinearities due to out-of-plane loads. (%)

Model	Load	max V	max W	max N	max|M_t|	max|M_y|	max|M_z|
1	EQ	5.7	8.2	3.0	8.6	17.8	10.4
	D + EQ	5.6	3.2	1.1	4.8	16.0	9.9
	W	4.9	8.7	3.2	7.2	16.1	6.9
	D + W	4.9	3.4	1.1	4.5	8.8	6.9
1*	EQ	4.9	6.3	2.6	5.2	15.7	1.2
	D + EQ	4.8	2.7	0.8	3.0	8.2	1.2
	W	4.3	7.5	3.0	4.5	14.5	5.8
	D + W	4.3	2.9	0.9	2.8	7.7	5.9

The comparison between the values for Model-1 and Model-1* shows that, if the rigidity of the slab is considered at the calculations, the nonlinearities will be reduced considerably, but the axial force in side ties will increase about 50%.

Elastic Buckling

To examine the out-of-plane stability of Model-1 and -2, a three-dimensional buckling analysis is carried out. The results are summarized in Table 5 in terms of α_{cr} values which are load multiples based on the intensity of design dead load. Model-1* and -2* denote the cases that the slab rigidities are taken into account, respectively for Model-1 and -2. In Table 5, the third mode of buckling of Model-1 and -1* alone is related to the out-of-plane buckling, and all of the other modes are to the in-plane buckling. Since, at ordinary rib arches, the first mode appears at the in-plane buckling and the second mode appears at the out-of-plane buckling, a solid-rib arch with side ties shows different behavior from the ordinary solid-rib arch at the higher order of buckling mode.

Table 5. Load multiples for out-of-plane buckling.

Model	1st mode	2nd mode	3rd mode
1	4.833	7.664	9.580
1*	5.215	8.243	9.914
2	2.677	5.097	8.153
2*	2.899	5.511	8.692

Ultimate Strength in In-Plane Loading

Ultimate Strength Analysis

By an elasto-plastic finite displacement analysis with a matrix method, the ultimate strength is calculated for the models of which an arch rib is divided into 832 elements. To discuss the characteristics in the ultimate state, six combined loads are applied as shown in Table 6. The inelastic behaviors are pursued in the numerical calculation until the unstable state. The yielding loads and the maximum loads obtained by the calculation are summarized in Table 6 in terms of load multiples α_y and α_{max}, respectively.

Table 6. Load multiples for yielding and maximum loads.

Model	α D		α (D + L)		D + α L	
	α_y	α_{max}	α_y	α_{max}	α_y	α_{max}
1	2.964	3.012	1.787	1.929	3.261	4.354
2	2.118	2.118	1.434	1.487	2.222	2.764
3 (10^{-4})	2.869	2.923	1.760	1.903	3.215	4.307
3 (10^{-3})	2.359	2.424	1.560	1.714	2.821	3.901

Model	α (D + EQ)		D + α EQ		1.3 D + α EQ	
	α_y	α_{max}	α_y	α_{max}	α_y	α_{max}
1	2.328	2.656	2.378	4.609	2.372	4.364
2	1.412	1.528	2.161	2.432	1.618	2.135
1*	2.690	2.723	4.199	6.050	4.120	4.737
2*	1.412	1.528	2.217	2.970	1.618	2.192

The values in the parentheses of Model-3 with an assumed initial imperfection, indicate the ratio of the maximum initial imperfection to the span length. The initial imperfections are determined from the buckling mode shown in Figure 8, which may be the most unfavorable mode under a uniform load. Model-1* and -2* are modification of Model-1 and -2, respectively, in which the same steel of *SM58* as the arch rib is used for ties, while at the actual bridge, *SM50Y* and *SS41* are used for the ties. *SM58*, *SM50Y* and *SS41* are structural steels specified at the Japanese Industrial Standards, respectively with the specified yielding point of 451, 353, 235 MPa (65.4, 51.2, 34.1 kipf/in^2), and the specified minimum tensile strength of 569, 490, 402 MPa (82.5, 71.1, 58.3 kipf/in^2).

Characteristic in Ultimate State

The comparison between the values for Model-1 and those for Model-2 in Table 6 proves the effectiveness of the side ties. If the arch is not provided with the both side ties, the arch will fail due to its elastic instability at a little greater load than the design dead load. The maximum values of initial imperfections used for the calculations are 1/1000 and 1/10000 of the span length corresponding to the amount of actual deflections of about 30 cm and 3 cm, respectively. Ohmishima Bridge will exhibit the amount of unavoidable initial imperfection between the both values. Table 6 shows that the reduction of ultimate strength due to the initial imperfections will be 2 to 3% for the case of 1/10000 and 10 to 11%

for the case of 1/1000, and also it will be 20% for the dead load alone. Therefore, the effect of initial imperfections on the ultimate strength of the actual bridge would be several percent and is much smaller than the one for an ordinary two-hinged solid-rib arch without side ties.

The typical relations between maximum deflections and various loadings are shown in Figures 9 and 10 at the nodal point No. 10. Elastic displacement curves by a finite displacement analysis and by a linear analysis as well as load versus displacement curves obtained by an elasto-plastic analysis, are presented in the figures. The figures show that any sudden instability after the maximum load does not occur for any Models. When the Models are subjected to a seismic load as well as the dead load, the first yielding is observed at ties. Therefore, at Model-1* and -2* which have ties in a steel of higher yielding point, the ultimate strength may be relatively larger depending on the loading, as proved in Table 6 and Figure 10.

Figure 9. Dead and live loads versus displacements (D + α L).

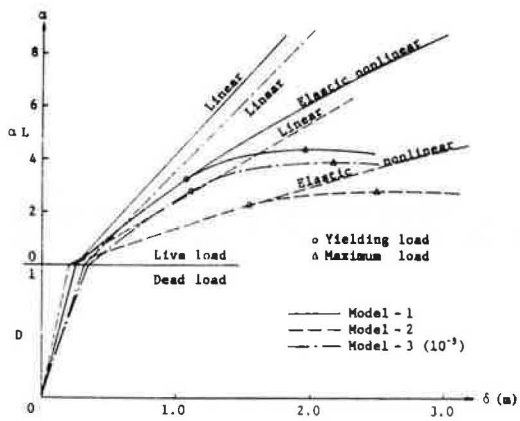

Figure 10. Dead and seismic loads versus displacements (D + α EQ).

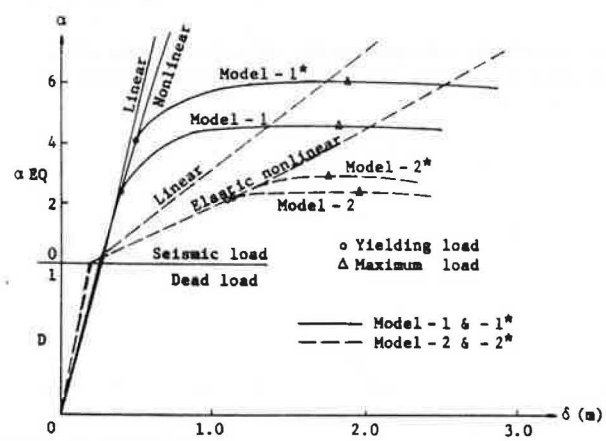

Note: 1 m = 3.28 ft.

Figures 11 and 12 present the spreading of plastic zone at the maximum load, but the members in which a plastic zone does not appear are omitted in the figures. In all of the loading cases, the arch rib fails due to its partial plastification, and particularly at Model-2, the arch rib fails without spreading of plastic zone after the yielding load has been reached.

Figure 11. Plastification due to dead load only (αD).

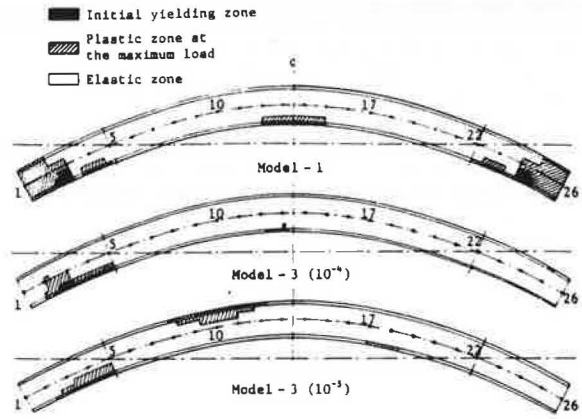

Figure 12. Plastification due to dead load plus seismic load (D + α EQ).

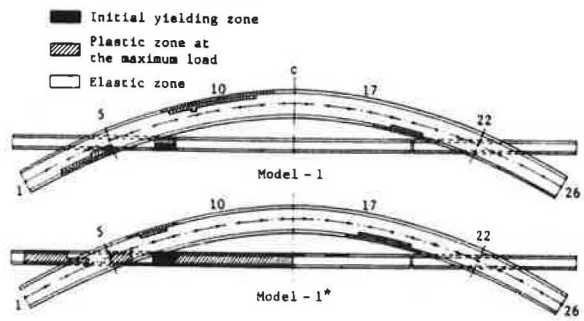

Ultimate Strength in Out-of-Plane Loading

At an elasto-plastic spatial analysis, the arch of Model-1 is divided into about 6000 elements and in addition to the dead load, wind load is applied to the arch rib, because it is dominant among possible out-of-plane loads.

Two kinds of ultimate strength are calculated, as shown in Table 7, in terms of the load multiple, α, for the maximum wind load. The comparison of Case-1 with Case-2 shows that 30% increase of the dead load, *D*, reduces slightly the strength for the wind load, *W*, because the model arch has a great in-plane strength for the dead load as shown in Table 6.

Table 7. Out-of-plane ultimate strength.

Loading	Case - 1 (1.0 D + α W)	Case - 2 (1.3 D + α W)
α_{max}	3.240	3.110

The relations between loads and out-of-plane displacements are given in Figure 13, in which the Nos. on the curves denote the nodal points of the leeward rib. The out-of-plane displacements at the nodal points of 31 and 33 differ about 2.5 times, although an interval between the both points is only two panel length. This difference is proper to an arch with side ties, because they constraint the out-of-plane displacements of arch ribs in side spans. Figure 15 which shows the out-of-plane displacements of arch ribs and ties, too, demonstrates clearly the effectiveness of the side ties.

Figure 13. Load versus displacement curves.

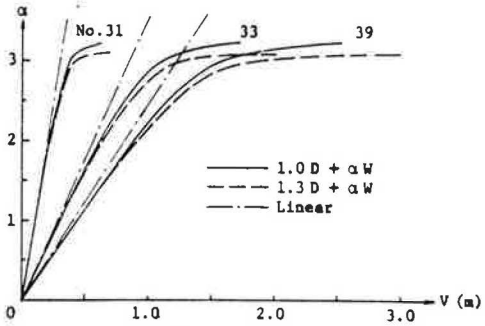

Note: 1 m = 3.28 ft.

Figure 14. Load versus out-of-plane moment curves.

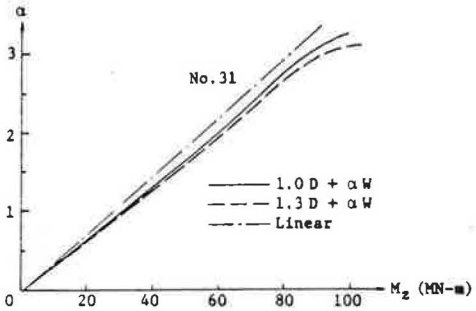

Note: 1 MN-m = 738 kip-ft.

Figure 14 indicates the relations of loads versus out-of-plane bending moments, M_z, at nodal point No. 31, at which the arch rib takes the maximum bending moment. The curves of out-of-plane bending moments in the rib do not show any remarkable nonlinearity as seen in Figure 14. Also, the nonlinearities in bending moments at the other sections are much smaller than those in displacements. The reason for these small nonlinearities in bending momments may be that, when the wind load reaches about 2.8 times as large as the design value, lateral braces between the arch ribs in the neighbourhood of the portal frames will yield and then the rapid displacements of the ribs will occur. Also, at the loading of $\alpha \simeq 3.0$, all of the sections of a great part of the side ties, too, yield, but at this time the greater parts of the ribs remain to be elastic.

Figure 15. Out-of-plane displacement distribution in arch rib and tie.

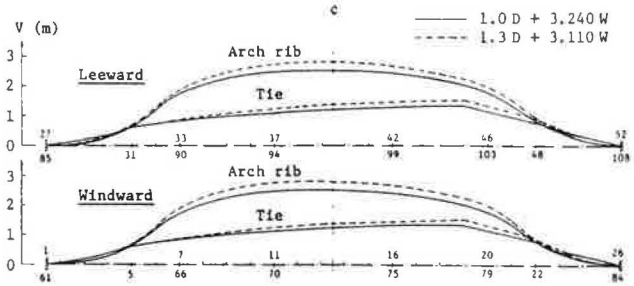

Note: 1 m = 3.28 ft.

Figure 16. Axial force distribution in arch rib for $(D + \alpha W)$.

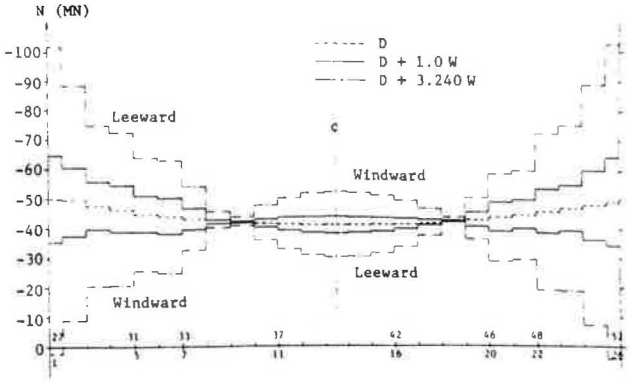

Note: 1 MN = 225 kip.

Figure 17. In-plane moment distribution in arch rib for $(D + \alpha W)$.

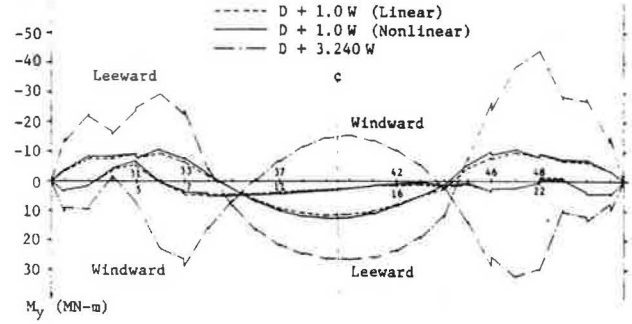

Figure 18. Out-of-plane moment distribution in arch rib for $(D + \alpha W)$.

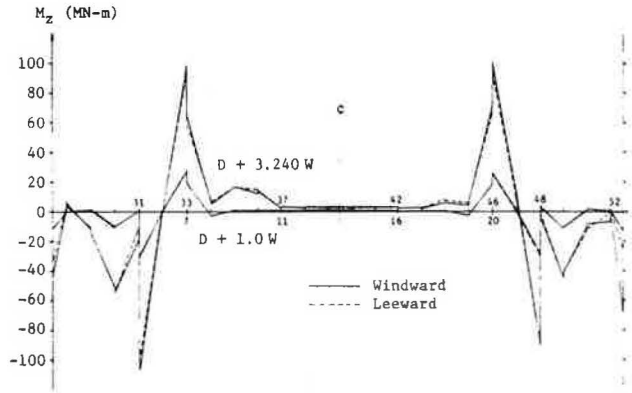

Note: 1 MN-m = 738 kip-ft.

At the model arch with the dimensions of Ohmishima Bridge, the structure reaches its unstable state due to the yielding of side ties and lateral braces around the portal frames. The plastification of the members at the maximum load is illustrated in Figure 19, but considerable portions of the members still remain to be elastic. All of the braces in the both side spans at floor systems not shown in Figure 19 will yield. If the plastic buckling of lateral braces between the ribs around the portal frames is taken into consideration in the numerical calculations, the values of α_{max} in Table 7 will be reduced to about 2.5.

Figure 19. Plastification of members at maximum load for $(D+\alpha W)$.

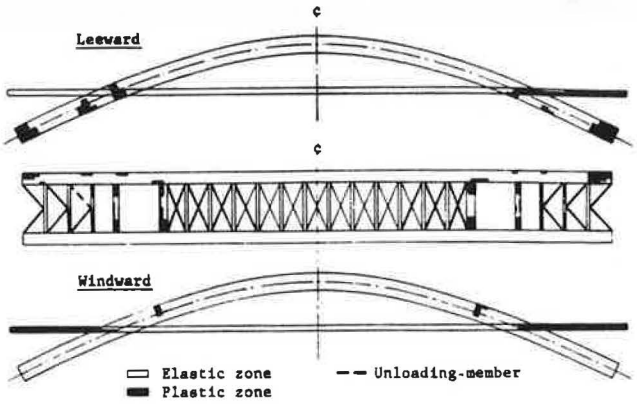

Finally, it should be added that experimental studies were carried out at Osaka University(2), and that six models in steel of a reduced scale of 1/49.5 for Ohmishima Bridge were tested to examine the in-plane and out-of-plane elasto-plastic behaviors and the ultimate strength. As the result, the ultimate strengths of the models by the theoretical analysis presented in this paper were verified quite well with 1 - 4% errors in comparison with the experimental values.

Conclusions

The theoretical and experimental analyses of two-hinged solid-rib steel arches stiffened by side ties modelling Ohmishima Bridge with the span length of 297 m, reveal the following structural characteristics:

1. The stiffening effects of side ties under in-plane loads are so remarkable that they can reduce the bending moments in arch ribs and also can constraint the geometrical nonlinearities of the arch, resulting in an increase of the load-carrying capacity of the overall structure.
2. Since the side ties can constraint the out-of-plane displacements of the arch ribs, they can increase the overall ultimate strength under out-of-plane loads.
3. Since it results that the span length of the arch rib has been shortened in appearance by the help of side ties, this new type of two-hinged arch will be more suitable for long-span arch bridges.

References

1. Honshu-Shikoku Bridge Authority. The Forth Working Design of Ohmishima Bridge, 1974 (in Japanese).
2. Y. Maeda, M. Hayashi and S. Matui. Study Report of Ohmishima Bridge - 1975 and 1976. Bridge Engineering Institute, Osaka University (in Japanese).
3. S.S. Tezcan and B.C. Mahapatra. Tangent Stiffness Matrix for Space Frame Members. ASCE, Vol. 95, No. ST 6, 1969, pp. 1257-1270.
4. K.H. Chu and R.H. Rampetsreiter. Large Deflection Buckling of Space Frames. ASCE, Vol.98, No. ST 12, 1972, pp. 2701-2722.
5. C. Oran. Tangent Stiffness in Space Frames. ASCE, Vol.99, No. ST 6, 1973, pp.987-1001.
6. Y. Maeda and M. Hayashi. Finite Displacement Analysis of Space-Framed Structures. Proc. of Japan Soc. of Civil Eng.(JSCE), 253, 1976, pp. 25-39 (in Japanese).
7. K. Washizu. Variational Methods in Elasticity and Plasticity. Pergamon Press, 1968, pp. 182-204.
8. Y. Yamada. Incremental Formulation for Problems with Geometric and Material Nonlinearities. Advances in Computational Methods in Structural Mechanics and Design. UAH Press, 1972, pp. 325-355.